Acta Biomaterialia 18 (2015) 206–212

Contents lists available at ScienceDirect

Acta Biomaterialia

journal homepage: www.elsevier.com/locate/actabiomat

# Statistical shear lag model – Unraveling the size effect in hierarchical composites

Xiaoding Wei, Tobin Filleter [1], Horacio D. Espinosa *

*Department of Mechanical Engineering, Northwestern University, 2145 Sheridan Road, Evanston, IL 60208-3111, USA*

ARTICLE INFO

*Article history:*
Received 29 August 2014
Received in revised form 8 December 2014
Accepted 28 January 2015
Available online 12 February 2015

*Keywords:*
Size effect
Load transfer
Shear lag
Defect tolerance
Hierarchical composites

ABSTRACT

Numerous experimental and computational studies have established that the hierarchical structures encountered in natural materials, such as the brick-and-mortar structure observed in sea shells, are essential for achieving defect tolerance. Due to this hierarchy, the mechanical properties of natural materials have a different size dependence compared to that of typical engineered materials. This study aimed to explore size effects on the strength of bio-inspired staggered hierarchical composites and to define the influence of the geometry of constituents in their outstanding defect tolerance capability. A *statistical* shear lag model is derived by extending the classical shear lag model to account for the statistics of the constituents' strength. A general solution emerges from rigorous mathematical derivations, unifying the various empirical formulations for the fundamental link length used in previous statistical models. The model shows that the staggered arrangement of constituents grants composites a unique size effect on mechanical strength in contrast to homogenous continuous materials. The model is applied to hierarchical yarns consisting of double-walled carbon nanotube bundles to assess its predictive capabilities for novel synthetic materials. Interestingly, the model predicts that yarn gauge length does not significantly influence the yarn strength, in close agreement with experimental observations.



## 1. Introduction

Hierarchical composite materials found in nature, such as nacre shells, collagen fibrils, and spider silk, are well known for their balanced strength and toughness [1–6]. Through staggered arrangements of constituents (i.e., strong and stiff filaments embedded in softer interfaces), natural composites can not only preserve the stiffness and strength of the filaments during material scale-up, but also achieve remarkable toughness. Microstructure characterizations of these natural composites reveal a critical length scale for each material that correlates to the two main failure mechanisms – filament fracture and interface sliding – to optimize macroscopic strength and toughness simultaneously [7–10]. Different continuum models have been advanced to relate critical length scales with mechanical properties of constituents, including key contributions by Gao et al. [11], Chen et al. [12], Rim et al. [13], Wei et al. [14], and Barthelat et al. [15]. Yet, these analyses were conducted on models that had assumed only a specified flaw with a predefined size and location. In practice, the location and size of flaws are randomly distributed along the strong and stiff filaments, and the number of flaw scales with the dimensions of filaments. Thus, the stochastic nature of flaw distribution needs to be taken into account in these continuum models. Following the pioneering work by Rosen and Zweben [16,17], various micromechanical models based on the weakest-link formulations have been proposed to predict strength distributions for unidirectional fiber-reinforced composites [18–24]. All of them assumed that the failure probability for an individual filament of length $L$ under stress $\alpha$ follows Weibull statistics is given by

$$P_f(\sigma, L) = 1 - \exp\left[-\frac{L}{L_0}\left(\frac{\sigma}{\sigma_0}\right)^m\right] \tag{1}$$

where $\sigma_0$ and $m$ are the scale and shape parameters, respectively, and $L_0$ is the reference filament length. Curtin proposed the characteristic strength $\sigma_c$ and length $L_c$ [23], defined by

$$\sigma_c = \left(\frac{\sigma_0^m \tau L_0}{r}\right)^{1/(m+1)} \quad \text{and} \quad L_c = \left(\frac{\sigma_0 r L_0^{1/m}}{\tau}\right)^{m/(m+1)} \tag{2}$$

where $r$ is the filament radius. Physically, $L_c$ is twice the length around a filament break that is required for the stress in the filament to recover linearly to the characteristic stress $\sigma_c$ with the assumption of a constant sliding resistance $\tau$ (i.e. $L_c = r\sigma_c/\tau$).

* Corresponding author.
*E-mail address:* espinosa@northwestern.edu (H.D. Espinosa).
[1] Current address: Department of Mechanical and Industrial Engineering, University of Toronto, 5 King's College Rd., Toronto, ON M5S 3G8, Canada.

http://dx.doi.org/10.1016/j.actbio.2015.01.040
1742-7061/

During studies of size effects in composite strength using statistical models [20,21,24–26], a fundamental link length $\hat{L}$ arose – it is the minimum link length below which the weakest-link scaling is *not applicable* to predict the strength distribution of a realistic composite with a total length $L_T \gg \hat{L}$. Phoenix et al. suggest $\hat{L} = \alpha L_c$ with $\alpha \sim 0.4$ [21], and Landis et al. suggest $\hat{L} = \beta\sqrt{3\pi E/Gr}$ with $\beta \sim 6$ and $E$ and $G$ are the elastic modulus and shear modulus of the filament and interface, respectively [25]. However, as noted in both reports, the coefficients $\alpha$ and $\beta$ may vary with the constituent mechanical properties and arrangements, so they have to be determined through intensive Monte Carlo simulations.

In this study, by introducing the statistical shear lag model, we developed a mathematical framework that yielded a more general formulation. This formulation solves the ambiguity in the fundamental link length scale and unifies the previous models. Moreover, the statistical shear lag model was implemented into a multiscale statistical model to explain how staggered hierarchical structures achieve superior flaw tolerance.

## 2. Statistical shear lag model

In our previous study, the classical shear lag model was used to describe the optimal length scale in staggered composites that simultaneously optimize their strength and toughness [14]. As shown in Fig. 1, a simplified 2D unit cell was constructed to study the load transfer efficiency between two adjacent filaments (with a thickness denoted as $b$) bonded by a thin soft interface layer (with a thickness denoted as $h$) over the length $L$. A tensile normal stress $\sigma_{app}$ is applied at the right end of the top filament, and the left end of the bottom filament is fixed in the axial direction but is free to deform in the lateral direction. The left end of the top filament and the right end of the bottom filament are traction-free and free to displace. Assuming the filaments and interface deform elastically, the solutions for axial tensile stress along the top and bottom filaments are expressed as

$$\begin{aligned} \sigma_1(x) &= \frac{\sigma_{app}}{\sinh\left(\frac{\lambda L}{2}\right)} \sinh\left(\frac{\lambda x}{2}\right) \cosh\left(\frac{\lambda(L-x)}{2}\right) \\ \sigma_2(x) = \sigma_1(L-x) &= \frac{\sigma_{app}}{\sinh\left(\frac{\lambda L}{2}\right)} \cosh\left(\frac{\lambda x}{2}\right) \sinh\left(\frac{\lambda(L-x)}{2}\right) \end{aligned} \tag{3}$$

respectively. In Eq. (3), $\lambda = \sqrt{\frac{2G}{Ehb}}$ in which $E$ is the elastic modulus of the filament and $G$ is the shear modulus of the interface.

Filament rupture and interface sliding were assumed to be the only two failure mechanisms that determine the composite strength. The classical shear lag model is based on several key assumptions. First, the filaments are treated as one-dimensional springs so that the transversal stress and variations in axial stress are neglected. Second, the interfaces carry no tensile but only shear load controlled solely by the relative displacements of filaments adhered to the interface regions. Microscopic characterizations suggest that the tensile strengths of reinforcements in natural composites spread widely due to variations in dominant defects [27]. In this study, we modified the classical shear lag model to account for the statistics in the tensile strength of reinforcements while keeping the key assumptions for the classical shear lag model.

Assuming the tensile strength of individual filaments follows the Weibull distribution function given by Eq. (1), the failure probability for a filament subject to a *nonhomogeneous* uniaxial stress state takes the integral form [28,29]:

$$P_f = 1 - \exp\left\{-\int_L \left[\frac{\sigma(\mathbf{x})}{\sigma_0}\right]^m \frac{dL(\mathbf{x})}{L_0}\right\}, \tag{4}$$

where $\sigma(\mathbf{x})$ is the distribution function of the effective uniaxial stress over the sample length $L$. Clearly, Eq. (4) suggests that both

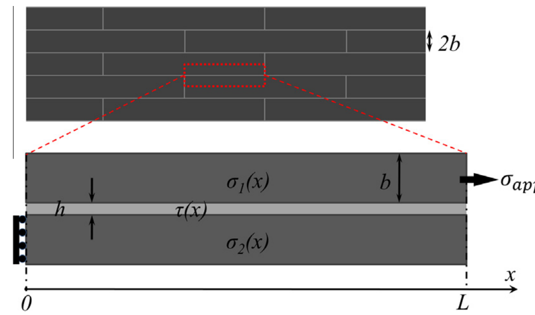


**Fig. 1.** Schematic of the 2D unit cell used in the statistical shear lag model simplified from the brick-and-mortar structure of a hierarchical staggered composite.

the material dimension and loading conditions affect the structural strength. Substituting Eq. (3) into Eq. (4), the probability of the rupture of any two filaments in the unit cell is given by

$$\begin{aligned} P_f(\sigma_{app}) &= 1 - \exp\left\{-\frac{2}{L_0}\int_0^L \left(\frac{\sigma_1(x)}{\sigma_0}\right)^m dx\right\} \\ &= 1 - \exp\left\{-\frac{2\int_0^L \left(\frac{1}{\sinh(\lambda L/2)}\cosh\left[\frac{\lambda}{2}(L-x)\right]\sinh\left(\frac{\lambda x}{2}\right)\right)^m dx}{L_0}\left(\frac{\sigma_{app}}{\sigma_0}\right)^m\right\} \end{aligned} \tag{5}$$

in which $L_0$ is the reference length for the filament in the simplified 2D unit cell. By defining the effective length

$$L_{eff}(L) = \int_0^L \left(\frac{1}{\sinh(\lambda L/2)}\cosh\left[\frac{\lambda}{2}(L-x)\right]\sinh\left(\frac{\lambda x}{2}\right)\right)^m dx, \tag{6}$$

we can rewrite Eq. (5) as

$$P_f(\sigma_{app}) = 1 - \exp\left\{-\frac{2L_{eff}}{L_0}\left(\frac{\sigma_{app}}{\sigma_0}\right)^m\right\}. \tag{7}$$

Eq. (7) suggests that the probability of the unit cell failing by filament rupture follows a Weibull distribution, which possesses the same shape parameter as the Weibull distribution of the monolithic filament rupture strengths. The new Weibull distribution for the rupture strength of the unit cell takes the form

$$P_f(\sigma_{app}) = 1 - \exp\left\{-\left(\frac{\sigma_{app}}{\sigma_{0,uc}}\right)^m\right\} \tag{8}$$

where $\sigma_{0,uc} = \sigma_0\left(\frac{L_0}{2L_{eff}}\right)^{1/m}$ is the scale factor for the unit cell rupture strength.

The statistical shear lag model introduced above facilitates the investigation of the statistics of unit cell rupture strengths as a function of overlap length. For a filament material whose strength has a Weibull distribution, the unit cell rupture strengths also follow Weibull statistics with a scale factor that is a function of the overlap length, as shown in Eqs. (6) and (8). The variance of the Weibull distribution for unit cell rupture strength is $\sigma_{0,uc}^2[\Gamma(1+2/m) - (\Gamma(1+1/m))^2]$. Alternatively, the unit cell can also fail by filament–filament sliding. For a linear elastic interface, the unit cell fails in sliding when $\sigma_{app} = 2\tau_f/(b\lambda)\tanh(\lambda L/2)$, in which $\tau_f$ is the interface shear strength [14]. Note that when scaling unit cells up to a macroscopic composite, the effective stress applied on the unit cell is $\sigma_{eff} = \sigma_{app}b/(2b+h)$. When the interface is thin (i.e., $h \ll b$), $\sigma_{eff}$ equals approximately $\sigma_{app}/2$.

To demonstrate the two competing failure mechanisms within the unit cell, a case study was performed on yarns made of double-walled carbon nanotube (DWCNT) bundles (see Fig. 2a) [30]. Each unit cell contains a pair of parallel DWCNT bundles. Statistics of bundle strength have been obtained through previous in situ SEM tensile experiments on 21 individual bundles with an average

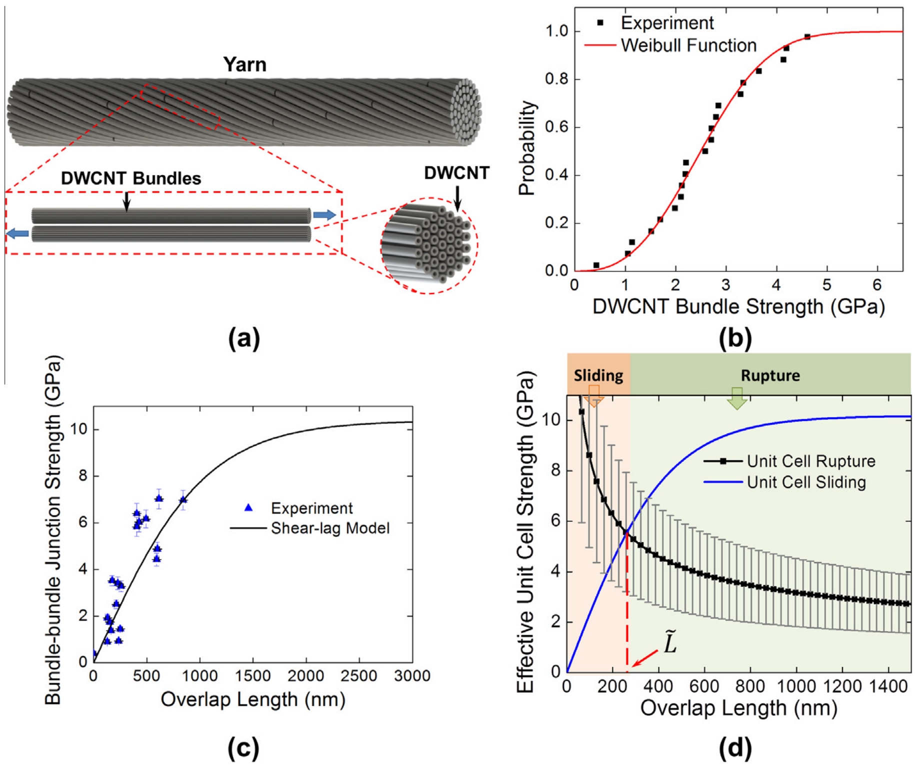


**Fig. 2.** (a) Schematic depicting the hierarchical structure of a macroscopic DWCNT yarn. Each unit cell in the yarn consists of two parallel DWCNT bundles. (b) Weibull analysis of the individual bundle rupture strength. (c) Simulated fit using the shear lag model of experimental shear strengths measured for two parallel DWCNT bundles. (d) Plot of the effective unit cell strength as a function of the unit cell length (overlap length). The unit cell strength determined by interface sliding is plotted in blue and by bundle rupture is plotted in black. Each black square represents the scale factor of the Weibull distribution function of the unit cell rupture strength at a particular overlap length. The error is the square root of the variance for each Weibull distribution function.

diameter of 25 nm and length of 5 μm [30–33]. After ordering 21 strength values ascendingly and defining $P_i = 100(i-0.5)/21$ as the sample percentile ($i = 1, \cdots, 21$), the set of strength values was fitted with the Weibull distribution function given by Eq. (1) to yield a scale factor of $\sigma_0 = 2.8$ GPa and a shape factor $m = 2.2$ (Fig. 2b). Note that the stress on a bundle in this study is defined as the load divided by the cross-sectional area of all carbon nanotube shells within the bundle. The mechanical properties of the interface were investigated through in situ SEM shear tests on pairs of parallel bundles [32]. A pair of bundles aligned parallel to one another with various overlap lengths was pulled on the opposite ends of the bundles with the force to break the junction recorded. As shown in Fig. 2c, tensile stresses required to slide 19 pairs of bundles were plotted as a function of overlap lengths. Previous coarse-grained simulations suggested that the interface between parallel bundles has a thickness $h \sim 2.5$ nm [32]. The equivalent filament thickness $b$ is approximated as half of the the bundle radius $r$. Fitting the results with the classical shear lag model solution $\sigma_{app} = 2\tau_f/(b\lambda)\tanh(\lambda L/2)$ yield an interface shear strength $\tau_f = 350$ MPa and an effective interface shear modulus $G = 10$ MPa. The properties of DWCNT bundles and interfaces are summarized in Table 1. Combining the results from the classical shear lag model and the statistical shear lag model, the effects of both failure modes on the unit cell strength are shown in Fig. 2d. The final unit cell strength is the smaller of the two strength values predicted by the statistical shear lag model and the classical shear lag model. The critical overlap length (or unit cell size) $\tilde{L}$ where the classical and statistical shear lag model solutions intersect gives the optimized unit cell strength and can be determined by numerically solving the following equation

$$\sigma_0\left(\frac{L_0}{2L_{eff}(\tilde{L})}\right)^{1/m} = \frac{2\tau_f}{b\lambda}\tanh\left(\frac{\lambda\tilde{L}}{2}\right). \tag{9}$$

For unit cells smaller than $\tilde{L}$, the scale factor $\sigma_{0,uc}$ fails to describe the unit cell strength due to the interface sliding, and thus is invalid for weakest-link model for size-scaling the composite strength. In other words, $\tilde{L}$ has the same physical meaning as the aforementioned fundamental link length $\hat{L}$. Moreover, we can show that Eq. (9) is a more general solution that can be simplified to the formulations proposed previously [21,25] under specific conditions.

When $m > 1$, the effective unit cell length $L_{eff}$ given by Eq. (6) is bounded by two limits

**Table 1**
Mechanical properties of DWCNT bundles and bundle–bundle interface.

| Bundle | Equivalent half filament thickness, $b$ (nm) | Elastic modulus, $E$ (GPa) | Strength scale factor, $\sigma_0$ (GPa) | Strength shape factor, m | Reference bundle length, $L_0$ (μm) |
|---|---|---|---|---|---|
| | 6.2 | 60 | 2.8 | 2.2 | 5 |
| Interface | Interface thickness, $h$ (nm) | Effective shear modulus, $G$ (MPa) | | Shear strength, $\tau_f$ (MPa) | |
| | 2.5 | 10 | | 350 | |

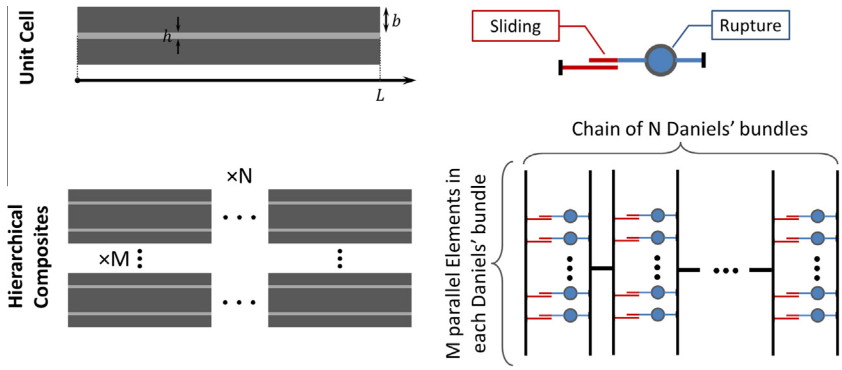


**Fig. 3.** Schematic of the method used to scale up the statistical shear lag model. The unit cell for the shear lag model (top left) is simplified as an element (top right) that has two failure modes (filament–filament sliding or filament rupture). A macroscopic hierarchical composite consisting of $M \times N$ unit cells (bottom left) is simplified into the statistical model of $M \times N$ elements (bottom right). The cross-section is represented in the axial direction as a chain of $N$ Daniel's bundles, and in the lateral direction as $M$ parallel elements.

$$\frac{L}{m+1} > L_{eff} > \frac{L}{2^m}. \tag{10}$$

$L_{eff}$ approaches the upper limit for a small $\lambda$ (meaning the interface is very soft compared to the filament) and approaches the lower limit for a large $\lambda$. Thus, for a small $\lambda$, Eq. (9) can be approximated as

$$\sigma_0\left(\frac{L_0(m+1)}{2\tilde{L}}\right)^{1/m} \approx \frac{\tau_f}{b}\tilde{L} \tag{11}$$

Solving Eq. (11) yields $\tilde{L} = \left[\frac{\sigma_0 b L_0^{1/m}}{\tau_f}\left(\frac{m+1}{2}\right)^{1/m}\right]^{m/(m+1)}$. Substituting the equivalent filament thickness $b \propto r/2$ for cylindrical filaments into this solution suggests that $\tilde{L}$ derived here has essentially the same functional form as the one proposed by Phoenix et al. with only a slight change in the coefficient [21]. It is clear that as $m$ decreases, a larger critical link length $\tilde{L}$ is required to apply weakest-link scaling. This is consistent with the observation in the Monte Carlo simulations by Landis et al. [25]. Similarly, for a large $\lambda$, Eq. (9) can be approximated as

$$\sigma_0\left(\frac{L_0 2^m}{2\tilde{L}}\right)^{1/m} \approx \frac{2\tau_f}{b\lambda} \tag{12}$$

Solving Eq. (12) yields another typical solution $\tilde{L} = \left(\frac{\sigma_0}{\tau_f}\sqrt{\frac{2Gb}{Eh}}\right)^m \frac{L_0}{2}$. This solution takes similar functional form as the one proposed by Landis et al., yet includes more constituent mechanical properties and geometries [25]. Therefore, through rigorous mathematical derivation, the statistical shear lag model developed herein provides a more general solution that solves the ambiguity in the fundamental link length scale obtained in previous statistical models for fiber-reinforced composites, bridging the gap between earlier theories.

## 3. Size effects in hierarchical composites

To extend the statistical shear lag model for evaluating the strengths of hierarchical composites, the following strategy was employed where the mechanical behavior of the unit cell was used as an input to investigate how the size of a macroscopic hierarchical composite is related to its strength. First, the unit cell (with length $L \geqslant \tilde{L}$) was simplified as an element consisting of two sub-elements connected in series; one sub-element represents filament rupture, and the other represents filament–filament sliding (see Fig. 3). Therefore, a hierarchical composite consisting of $M \times N$ unit cells can be simplified into the statistical model consisting of $M \times N$ elements. The cross-section of the composite is modeled as a Daniels' bundle of $M$ parallel unit cells aligned in the lateral direction that are evenly clamped at both ends [34]. Along the axial direction, the composite is simplified as a chain of N Daniels' bundles connected in series such that the composite has a total length $L_{comp} = N \cdot L$. Daniels' theory suggests that the strength of a bundle consisting of $M$ unit cells whose strength distribution is a Weibull probability function exhibits a Gaussian distribution expressed as

$$\begin{aligned} &G(\sigma_{eff}) = \tfrac{1}{2}\left[1 + erf\left(\tfrac{\sigma_{eff}-\mu}{\sqrt{2\delta^2}}\right)\right] \\ &\text{in which,} \\ &\mu = \left(\tfrac{1}{m}\right)^{\frac{1}{m}} \exp\left(-\tfrac{1}{m}\right)\sigma_{0,eff}, \\ &\delta^2 = \tfrac{1}{M}\left(\tfrac{1}{m}\right)^{\frac{2}{m}} \exp\left(-\tfrac{1}{m}\right)\left[1 - \exp\left(-\tfrac{1}{m}\right)\right](\sigma_{0,eff})^2, \text{ and} \\ &\sigma_{0,eff} = \sigma_{0,un}\tfrac{b}{(2b+h)} \end{aligned} \tag{13}$$

The strength of a composite consisting of $N$ serially connected Daniels' bundles is governed by the weakest bundle and thus is distributed as

$$H(\sigma_{eff}) = 1 - [1 - G(\sigma_{eff})]^N. \tag{14}$$

As shown by Phoenix and Raj [19], the Weibull approximation to $H(\sigma_{eff})$ takes the form

$$H(\sigma_{eff}) \approx 1 - \exp\left[-\left(\frac{\sigma}{\sigma'}\right)^{m'}\right], \tag{15a}$$

with the composite Weibull scale factor $\sigma'$ given by

$$\sigma' = \mu + \delta\left[\frac{\log(\log(N)) + \log(4\pi)}{\sqrt{8\log(N)}} - \sqrt{2\log(N)}\right], \tag{15b}$$

and the composite shape factor $m'$ given by

$$m' = \frac{\mu\sqrt{2\log(N)}}{\delta} + 2\left[\frac{\log(\log(N)) + \log(4\pi)}{\sqrt{2\log(N)}} - \log(N)\right]. \tag{15c}$$

## 4. Results

Clearly, there is a size effect with respect to the strength of composites with different hierarchies as a function of the filament material (Eq. (1)), the unit cell (Eqs. 6–8), and the composite size (Eqs. (13), (14), (15a), (15b), (15c)). To illustrate this size effect, a case study was performed on a DWCNT yarn consisting of unit cells with an overlap length of 2.5 μm. The yarn contained $10^3$ elements in the lateral direction and $10^6$ Daniels' bundles in the axial

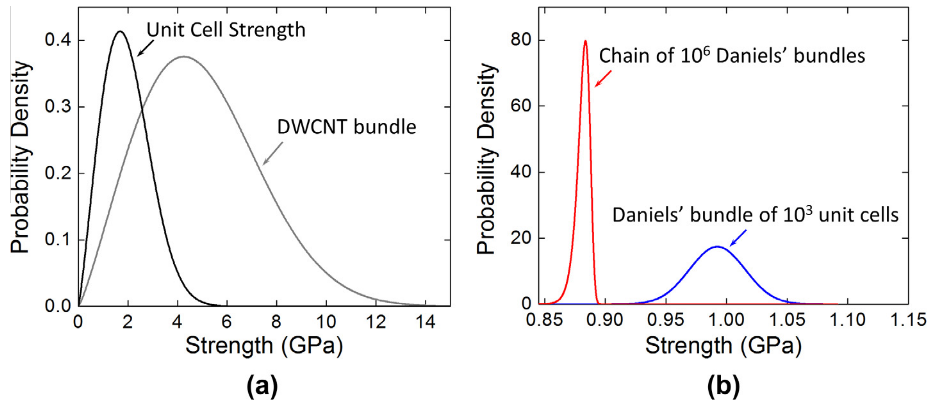


**Fig. 4.** Probability density functions for different hierarchies in the DWCNT yarn. (a) The probability density functions of the DWCNT bundle rupture strength and unit cell strength obtained from Eqs. (1) and (8); (b) the probability density functions of the Daniels' bundle strength (consisting of $10^3$ unit cells) and the macroscopic yarn strength (consisting of $10^6$ Daniels' bundles) obtained from Eqs. (13) and (14).

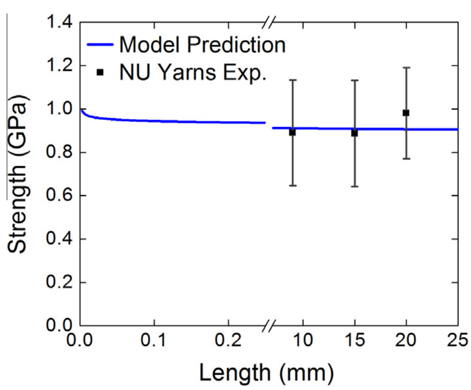


**Fig. 5.** The predicted strength of the hierarchical DWCNT yarns as a function of yarn length demonstrates the suppressed length scale sensitivity. Experimentally measured DWCNT yarn strength at various gauge lengths are included to compare with the model prediction (the error represents the standard deviation of yarn strength).

direction. Fig. 4 shows the probability density distributions for the strengths of 2.5 μm long and 30 nm diameter DWCNT bundle, a unit cell, Daniels' bundle of $10^3$ elements (with a diameter of approximately 30 μm), and a chain of $10^6$ Daniels' bundles (i.e. a 2.5 m long yarn). The Weibull distributions for DWCNT bundles and unit cells share the same shape factor, while the scale factor for the unit cell strength is lower than that for the DWCNT bundle strength. The strength of the yarn's cross section shows a Gaussian distribution. In contrast, the strength distribution of a chain of $10^6$ Daniels' bundles exhibits a Weibull distribution function profile. Fitting the data yields a scale factor of approximately 0.9 GPa and a very high shape factor of 195, in excellent agreement with the Weibull approximation (0.9 GPa and 203) given by Eqs. (15b) and (15c). This much higher shape factor as compared with that of 2.2 for individual DWCNT bundles indicates an increase in reliability as yarn length increases, which is consistent with previous reports [24].

More interestingly, the statistical model explains why a hierarchical structure is so important in material scaling up – from

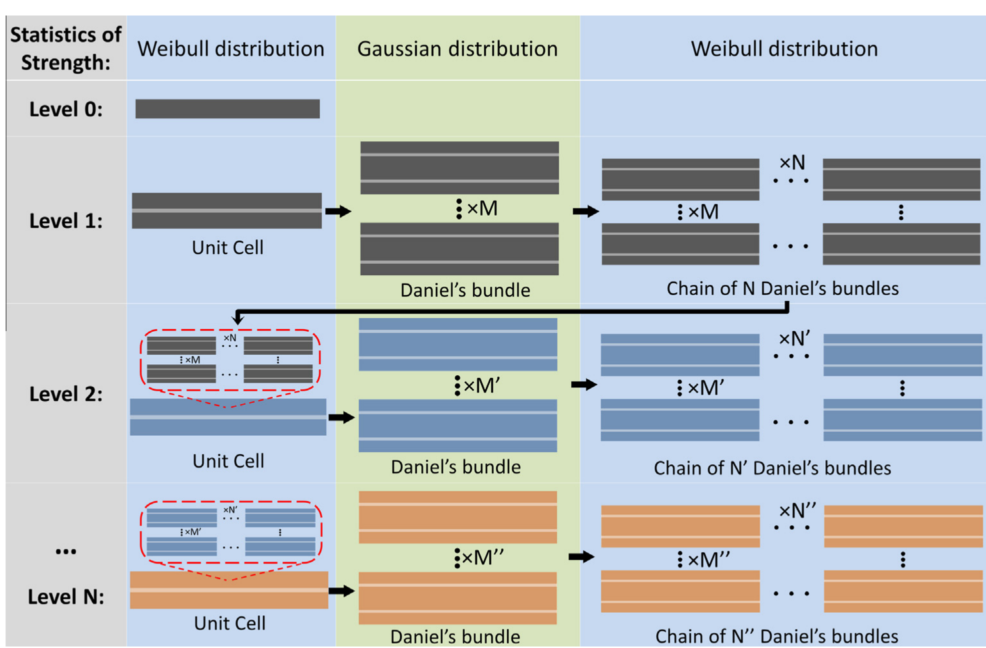


**Fig. 6.** Schematic representation of multi-level hierarchical composites exhibiting a transition of strength statistics from Weibull to Gaussian to Weibull, at each hierarchical level, during material scaling-up.

nanoscale constituents to macroscopic composites. Fig. 5 shows that the mean strength value for the DWCNT yarn (a discontinuous hierarchical composite) depends barely on the yarn length – when the yarn length increases by $10^4$ times (from 2.5 μm to $2.5 \times 10^4$ μm), the mean yarn strength drops by only 10% (from 1 to 0.9 GPa). The model prediction agrees very well with the results of tensile experiments on DWCNT yarns [35]. The experimentally measured mean strengths at various yarn gauge lengths agree with the model predictions and do not show appreciable length dependence. Insensitivity of strength with respect to gauge length has also been observed in other composites containing natural or synthetic fibers, such as sisal fibers and carbon fibers [26,36,37], as they share the same deformation mechanisms. By obtaining the mechanical properties of the constituents through micromechanical experiments, this model could potentially be applied to those composites to gain further insights into the microstructure–property relationships. Thus, understanding why the hierarchical structures are common in most of the natural composites is straightforward – through this approach, which reveals the ability of discontinuous staggered composites to re-distribute load over characteristic length scales that are functions of constituent geometry and mechanical properties. Hence, macroscopic natural composites can preserve remarkable mechanical properties when scaling up from the filaments usually in the nm or μm length scales.

## 5. Discussion

Finally, it is worth to note that the statistical models previously introduced can be applied to composites with nested hierarchical structures (as shown in Fig. 6). With the strength of the building block at level 0 following a Weibull distribution, based on the above result, at level 1 the statistics of strength starts with a Weibull distribution for the unit cell, then transitions to a Gaussian distribution when the material scales in the lateral direction, and finally returns to a new Weibull distribution when the material scales in the axial direction (to form a fibril). It is obvious that the fibril at the end of the hierarchical level 1 serves as reinforcement for the unit cell at level 2. According to the statistical shear-lag model, the strength of the unit cell at level 2 should follow a Weibull distribution as well. Replicating this procedure suggests that this Weibull–Gaussian–Weibull distribution transition repeats at each hierarchical level according to Eqs. 6, 7, 8, 13, 14, 15a, 15b and 15c. Therefore, the statistical model developed in the current study is a self-consistent multi-scale model that can predict the mechanical strength of bio-inspired hierarchical composites and reveal the unique size-effect on the mechanical strength that benefits from the staggered hierarchical structure. We note that the statistical shear lag model introduced here assumed an ideally parallel alignment of filaments. In the future, effects of filament bending and torsion will be taken into account so that the model can be applied to composites that have more complicated microstructures (e.g., CNT ropes containing hierarchical helical microstructures) [38].

## 6. Concluding remarks

In the current study, the statistical shear lag model was extended to investigate the size effect on the hierarchical composites' mechanical properties at all levels including the filaments, unit cell, and the macroscopic composite. The model suggests that the statistics of the filament strength plays an important role in the optimization of the geometries of the unit cell. A more general solution emerged for the critical link length scale beyond which the Weibull analysis can be applied to predict size scaling of composite strength. This solution unifies the formulations proposed in previous statistical models that were determined empirically. Furthermore, the multiscale statistical model shows that the staggered composites have suppressed size-dependent mechanical properties. This multiscale statistical model reveals the transition of the statistics of strength during material scaling-up at each level in a composite with nested hierarchical structures. By factoring discontinuities into the composites in a controlled manner, staggered composites can achieve an incredible capability for defect tolerance due to their hierarchical structures. This finding provides valuable insights for the design of novel bio-inspired high-performance composite materials. For example, with reasonable modifications to account for the difference in geometries of building blocks, this statistical model can be applied to other nanocomposites, such as laminated graphene oxide-polymer composites, to guide the microstructure design that preserves the excellent mechanical properties of the nanoscale building blocks [39–41].

## Acknowledgements

The authors acknowledge support from ARO through MURI award W911NF-09-1-0541 and the NSF through DMREF award CMMI-1235480. The authors also thank Matthew Ford for assistance in equation derivation and discussions.

## Appendix A. Figures with essential colour discrimination

Certain figures in this article, particularly Figs. 1–6, are difficult to interpret in black and white. The full colour images can be found in the on-line version, at http://dx.doi.org/10.1016/j.actbio.2015.01.040.

## References

[1] Currey J. Mechanical properties of mother of pearl in tension. Proc R Soc Lond B Biol Sci 1977;196:443–63.
[2] Barthelat F, Tang H, Zavattieri P, Li C-M, Espinosa H. On the mechanics of mother-of-pearl: a key feature in the material hierarchical structure. J Mech Phys Solids 2007;55:306–37.
[3] Fratzl P, Misof K, Zizak I, Rapp G, Amenitsch H, Bernstorff S. Fibrillar structure and mechanical properties of collagen. J Struct Biol 1998;122:119–22.
[4] Keten S, Xu Z, Ihle B, Buehler MJ. Nanoconfinement controls stiffness, strength and mechanical toughness of [beta]-sheet crystals in silk. Nat Mater 2010;9:359–67.
[5] Espinosa HD, Rim JE, Barthelat F, Buehler MJ. Merger of structure and material in nacre and bone – perspectives on *de novo* biomimetic materials. Prog Mater Sci 2009;54:1059–100.
[6] Espinosa HD, Juster AL, Latourte FJ, Loh OY, Gregoire D, Zavattieri PD. Tablet-level origin of toughening in abalone shells and translation to synthetic composite materials. Nat Commun 2011;2:173.
[7] Meyers MA, Lin AY-M, Chen P-Y, Muyco J. Mechanical strength of abalone nacre: role of the soft organic layer. J Mech Behav Biomed Mater 2008;1:76–85.
[8] Landis W, Song M, Leith A, McEwen L, McEwen B. Mineral and organic matrix interaction in normally calcifying tendon visualized in three dimensions by high-voltage electron microscopic tomography and graphic image reconstruction. J Struct Biol 1993;110:39–54.
[9] Penel S, Morrison RG, Dobson PD, Mortishire-Smith RJ, Doig AJ. Length preferences and periodicity in β-strands. Antiparallel edge β-sheets are more likely to finish in non-hydrogen bonded rings. Protein Eng 2003;16:957–61.
[10] Shao Y, Zhao H-P, Feng X-Q, Gao H. Discontinuous crack-bridging model for fracture toughness analysis of nacre. J Mech Phys Solids 2012;60:1400–19.
[11] Gao H, Ji B, Jäger IL, Arzt E, Fratzl P. Materials become insensitive to flaws at nanoscale: lessons from nature. Proc Natl Acad Sci 2003;100:5597–600.
[12] Chen B, Wu P, Gao H. A characteristic length for stress transfer in the nanostructure of biological composites. Compos Sci Technol 2009;69:1160–4.
[13] Rim JE, Zavattieri P, Juster A, Espinosa HD. Dimensional analysis and parametric studies for designing artificial nacre. J Mech Behav Biomed Mater 2011;4:190–211.
[14] Wei X, Naraghi M, Espinosa HD. Optimal length scales emerging from shear load transfer in natural materials: application to carbon-based nanocomposite design. ACS Nano 2012;6:2333–44.
[15] Barthelat F, Dastjerdi AK, Rabiei R. An improved failure criterion for biological and engineered staggered composites. J R Soc Interface 2013;10:20120849.
[16] Rosen BW. Tensile failure of fibrous composites. AIAA J 1964;2:1985–91.
[17] Zweben C. Tensile failure of fiber composites. AIAA J 1968;6:2325–31.
[18] Curtin WA. Theory of mechanical properties of ceramic-matrix composites. J Am Ceram Soc 1991;74:2837–45.

[19] Phoenix S, Raj R. Overview no. 100 scalings in fracture probabilities for a brittle matrix fiber composite. Acta Metall Mater 1992;40:2813–28.
[20] Curtin W, Takeda N. Tensile strength of fiber-reinforced composites: II. Application to polymer matrix composites. J Compos Mater 1998;32:2060–81.
[21] Phoenix S, Ibnabdeljalil M, Hui C-Y. Size effects in the distribution for strength of brittle matrix fibrous composites. Int J Solids Struct 1997;34:545–68.
[22] Batdorf S, Ghaffarian R. Size effect and strength variability of unidirectional composites. Int J Fract 1984;26:113–23.
[23] Curtin W. Ultimate strengths of fibre-reinforced ceramics and metals. Composites 1993;24:98–102.
[24] Ibnabdeljalil M, Curtin W. Strength and reliability of fiber-reinforced composites: localized load-sharing and associated size effects. Int J Solids Struct 1997;34:2649–68.
[25] Landis CM, Beyerlein IJ, McMeeking RM. Micromechanical simulation of the failure of fiber reinforced composites. J Mech Phys Solids 2000;48:621–48.
[26] Okabe T, Takeda N. Size effect on tensile strength of unidirectional CFRP composites—experiment and simulation. Compos Sci Technol 2002;62:2053–64.
[27] Menig R, Meyers MH, Meyers MA, Vecchio KS. Quasi-static and dynamic mechanical response of *Haliotis rufescens* (abalone) shells. Acta Mater 2000;48:2383–98.
[28] Bazant ZP, Planas J. Fracture and size effect in concrete and other quasibrittle materials. CRC press; 1997.
[29] Bažant Z. Size effect on structural strength: a review. Arch Appl Mech 1999;69:703–25.
[30] Naraghi M, Filleter T, Moravsky A, Locascio M, Loutfy RO, Espinosa HD. A multiscale study of high performance double-walled nanotube – polymer fibers. ACS Nano 2010;4:6463–76.
[31] Filleter T, Bernal R, Li S, Espinosa H. Ultrahigh strength and stiffness in cross-linked hierarchical carbon nanotube bundles. Adv Mater 2011;23:2855–60.
[32] Naraghi M, Bratzel GH, Filleter T, An Z, Wei X, Nguyen ST, et al. Atomistic investigation of load transfer between DWNT bundles "Crosslinked" by PMMA oligomers. Adv Funct Mater 2013;23:1883–92.
[33] Papkov D, Beese AM, Goponenko A, Zou Y, Naraghi M, Espinosa HD, et al. Extraordinary improvement of the graphitic structure of continuous carbon nanofibers templated with double wall carbon nanotubes. ACS Nano 2012;7:126–42.
[34] Daniels H. The statistical theory of the strength of bundles of threads. I. Proc R Soc Lond A Math Phys Sci 1945;183:405–35.
[35] Beese AM, Wei X, Sarkar S, Ramachandramoorthy R, Roenbeck MR, Moravsky A, et al. Key factors limiting carbon nanotube yarn strength: exploring processing–structure–property relationships. ACS Nano 2014;8:11454–66.
[36] Silva FdA, Chawla N. Tensile behavior of high performance natural (sisal) fibers. Compos Sci Technol 2008;68:3438–43.
[37] Pickering K, Murray T. Weak link scaling analysis of high-strength carbon fibre. Compos A Appl Sci Manuf 1999;30:1017–21.
[38] Zhao Z-L, Zhao H-P, Wang J-S, Zhang Z, Feng X-Q. Mechanical properties of carbon nanotube ropes with hierarchical helical structures. J Mech Phys Solids 2014;71:64–83.
[39] Stankovich S, Dikin DA, Dommett GH, Kohlhaas KM, Zimney EJ, Stach EA, et al. Graphene-based composite materials. Nature 2006;442:282–6.
[40] Beese AM, An Z, Sarkar S, Nathamgari SSP, Espinosa HD, Nguyen ST. Defect-tolerant nanocomposites through bio-inspired stiffness modulation. Adv Funct Mater 2014;24:2883–91.
[41] Suk JW, Piner RD, An J, Ruoff RS. Mechanical properties of monolayer graphene oxide. ACS Nano 2010;4:6557–64.